

# 4D characterization of metals by 3DXRD

**Poulsen, Henning Friis; Ludwig, W.; Lauridsen, Erik Mejdal; Schmidt, Søren; Pantleon, Wolfgang; Olsen, Ulrik Lund; Oddershede, Jette; Reischig, P.; Lyckegaard, Allan; Wright, J.**

*Total number of authors:*
11

*Published in:*
Proceedings of the Risø International Symposium on Materials Science

*Publication date:*
2010

*Document Version*
Publisher's PDF, also known as Version of record

Proceedings of the 31st
Risø International Symposium on Materials Science:
*Challenges in materials science and possibilities*
*in 3D and 4D characterization techniques*
Editors: N. Hansen, D. Juul Jensen,
S.F. Nielsen, H.F. Poulsen and B. Ralph
Risø National Laboratory for Sustainable Energy,
Technical University of Denmark, 2010

# 4D CHARACTERIZATION OF METALS BY 3DXRD

H.F. Poulsen[*], W. Ludwig[†§], E.M. Lauridsen[*], S. Schmidt[*], W. Pantleon[*], U.L. Olsen[*], J. Oddershede[*], P. Reischig[†‡], A. Lyckegaard[*], J. Wright[†], G. Vaughan[†].

*Center for Fundamental Research: Metal structures in Four Dimensions, Risø DTU, Frederiksborgvej 399, 4000 Roskilde, Denmark
†European Synchrotron Radiation Facility, 6 Rue Jules Horowitz, 38043 Grenoble, France
§Université de Lyon, MATEIS, UMR5510, CNRS, France
‡ Institute for Synchrotron Radiation, Karlsruhe Institute of Technology, Germany

## ABSTRACT

The status of 3DXRD microscopy is reviewed, with a special view to applications in metallurgy. Various approaches are compared in terms of performance. In addition several recent advances are presented, such as a 3D grain map with an unprecedented spatial resolution of 500 nm, first results from the commissioning of a novel 3D detector set-up and a validation of the box-scan procedure.

## 1. INTRODUCTION

Three-Dimensional X-Ray Diffraction (3DXRD) is a novel technique, aiming at a fast and non-destructive characterization of the individual crystalline elements within mm-sized poly-crystalline specimens. It is based on two principles: the use of highly penetrating hard X-rays from a synchrotron source (x-ray energies in the range 20-100 keV) and the application of "tomographic" reconstruction algorithms for the analysis of the diffraction data. In favourable cases, the position, morphology, phase, and crystallographic orientation can be derived for hundreds of elements simultaneously as well as their elastic strains. Furthermore, the dynamics of the individual elements can be monitored during typical processes such as deformation or annealing. Hence, for the first time information on the interaction between elements can be obtained directly. The provision of such data is vital in order to extend beyond state-of-art structural models.

Notably, in a 3DXRD experiment one must prioritise between spatial, angular and time resolution. This has lead to a variety of 3DXRD strategies, which we in the following will summarise as three standard modes of operation. The first mode, grain centre mapping, enables fast measurements of the *average characteristics* of each grain - such as their centre-of-mass position, volume, average orientation, dislocation density and/or average strain tensor - while

the exact location of the grain boundaries is unknown. The second mode enables full 3D mappings of grains and orientations. The third mode relates to work on more extended specimens (or the use of bulky sample surroundings) and involves a slower data acquisition rate.

In the following, initially the two most common 3DXRD setups will be presented and recent advances in instrumentation are discussed. Following this the standard modes of operation are presented in more detail with selected examples of use. For general reference, a mathematical description of the methodology and additional applications, see (Poulsen 2004, Poulsen 2009). In terms of selection of examples, there will be a bias towards work in Europe. A complementary report on the status in US is given by Lienert, Brandes, Bernier, Mills, Miller, Li, Hefferan, Lind, and Suter (2010). More recently, new approaches have been demonstrated with the aim of generalising the concepts of 3DXRD and X-ray diffraction imaging, as well as extensions of 3DXRD into the nano-scale. Some of these will be presented in the accompanying articles in these proceedings by Ludwig, Reischig, King, Herbig, Proudhon, Buffiere, Rutishauser and David (2010), King, Reischig, Martin, Fonseca, Preuss, and Ludwig (2010), and Vaughan, Wright, Bytchkov, Curfs, Gundlach, Orlova, Erra, Gleyzolle, Buslaps, Götz, Suchet, Petitdemange, Rossat, Margulies, Ludwig, Snigirev, Snigireva, Schmidt, Sørensen, Lauridsen, Olsen, Oddershede, and Poulsen (2010).

Alternative approaches to provision of 3D maps based on X-ray diffraction exist. These are based on inserting wires (Larson, Yang, Ice, Budai, and Tischler 2002), slits (Bunge, Wcislak, Klein, Garbe, and Schneider 2003) or collimators (Wroblewski, Clauss, Crostack, Ertel, Fandrich, Genzel, Hradil, Ternes, and Woldt 1999) between the sample and the detector and scanning the sample with respect to these elements. Not surprisingly such methods will be slower than the tomographic approach of 3DXRD, but they may be associated with other advantages, such as improved options for measuring the local elastic strain. In particular we mention the technique of "differential-aperture X-ray microscopy" (Ice, Larson, Yang, Budai, Tischler, Pang, Barabash, and Liu 2005). Using a polychromatic microbeam with energies of 8-20 keV and scanning a wire, a 200 nm resolution in 3D has been demonstrated. For recent examples of applications see elsewhere in these proceedings (Ice and Pang 2010; Barabash, Tischler, Ice, and Barabash 2010).

Another related effort is the work by Bleuet, Welcomme, Dooryhee, Susini, Hodeau, and Walter (2008) on probing the structure of heterogeneous diluted materials by diffraction tomography. Using a pencil beam and scanning the sample, this is a powerful technique for instance to map the spatial distribution of crystallographic phases (but not individual grains) in small grained, multiphase materials.

## 2. EXPERIMENTAL SET-UP

Currently there are three dedicated 3DXRD microscopy set-ups: two permanent installations at beamline ID11 at the European Synchrotron Radiation Facility (ESRF) in Grenoble and at beamline 1-ID at the Advanced Photon Source (APS) in Chicago, respectively, and a mobile set-up - built by Ludwig - which has been used at several beamlines at ESRF. The mobile set-up is different in several aspects and the associated technique is also known as *diffraction contrast tomography* (DCT).

The *set-up for the two permanent microscopes* – as well as an upcoming one at PETRA-III, Hamburg - is sketched in Fig 1. A parallel and monochromatic beam of X-rays emerging from the synchrotron illuminates an extended part of the sample. If the full sample is illuminated, typically a complete 3D mapping requires data acquisition while rotating around one axis

perpendicular to the beam – the ω-axis in Fig 1. If only a 2D cross-section is illuminated, one needs in addition to scan the sample in z and stack the results from the individual layers. The transmitted beam is monitored by a set of (semi-transparent) 2D detectors, placed at different distances to the sample. Depending on the science case at hand and the dimensions of sample and optional auxiliaries, one or more of these detectors may be translated out of the beam-path.

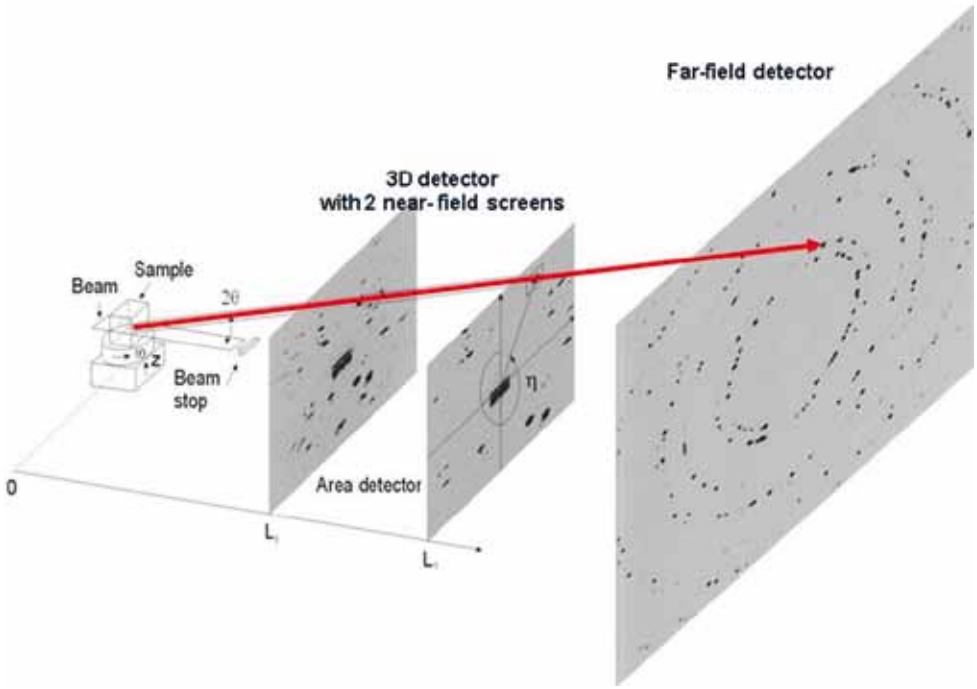


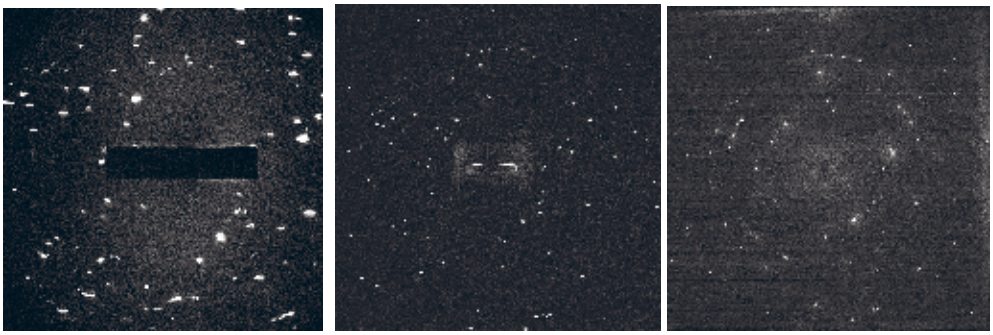

Fig 1. Top: 3DXRD set-up used at ID11, ESRF. The angles 2θ, ω and η are defined. Below: Examples of raw images acquired with the 3D detector. The sample is an annealed Al1050 polycrystal with grains of average size 70 μm. The X-ray energy was 55 keV. Left is the inner-most screen at a distance of 7 mm from the sample, middle is the second screen at a distance of 17 mm, and right is the far-field detector at a distance of 190 mm.

As an example, we provide more detailed information on the set-up at ID11. Here recently a so-called 3D detector unit has been installed, comprising two near-field 2D detectors. Both of these

comprise a scintillator screen, which converts X-rays to visual photons. Via a mirror and conventional microscope optics, the visual light is acquired by a CCD. The scintillators are 30μm thick freestanding LuAG(Te) foils with 7% absorption at 50keV. The 3D detector is designed such that the first screen is at a distance of 3-10 mm from the sample, while the distance between the first and second screen is fixed at 10 mm. The pixel size of the two screens are 1.5 and 4.5 μm, and the corresponding active areas are $(3.072\ \text{mm})^2$ and $(9.216\ \text{mm})^2$, respectively. The far-field detector is a FRELON camera. Positioned at a distance of 20-40 cm from the sample it has a pixel size of 50 μm and an active area of $(102.4\ \text{mm})^2$. These three detectors all probe the dark field diffracted beam. The two screens and mirrors in the 3D detector have a small hole in the centre that allows the direct beam to pass through to be detected by a high-resolution camera, which probe the attenuation of the direct beam - not shown in Fig 1. This is used for simultaneous absorption and phase contrast tomography.

An example of raw data is shown in Fig 1. On the innermost detector, the diffraction spots are distributed almost randomly, and the position and shape reflects the position and morphology of the associated grain. Hence, this detector essentially provides the spatial resolution. On the far-field detector, the diffraction spots are positioned on the Debye-Scherrer ring familiar from powder diffraction. In this case there is essentially no spatial information in the pattern, but a high angular resolution, ideal for stress characterization and crystallography. The detector at intermediate distance serves to provide additional data, adding robustness to the reconstruction algorithms and provides new possibilities, e.g. for making use of ray-tracing principles. One drawback of this set-up is that all detectors need very careful alignment and calibration. Another is that the efficiency of all 3 detectors is energy dependent and furthermore the ratio of peak intensities between the 3 detectors varies with the mosaicity and crystal size of the sample. Hence, exposure times must be carefully decided to obtain a useful signal on all detectors simultaneously.

The *DCT set-up* is based on a different approach, as sketched in Fig 2. In this case only one (near-field) detector is used. The direct beam is made to have dimensions, which imply that it illuminates a square in the center of the detector, comprising approximately 10% of the total detector area. In this way, absorption contrast tomography, extinction spots and diffraction spots can all be seen in the same image - see the example in Fig 2 - and furthermore a standard tomography detector can be used. This makes the set-up more robust, and currently the 3D maps with the highest spatial resolution are made in this way. On the other hand, the set-up is less versatile; in particular there are fewer options for crystallography.

Independent of which set-up is used, the task at hand is from such a set of data to perform the 3D reconstruction of the microstructural features of interest.

## 3. GRAIN CENTER MAPPING

An important simplification arises in the case where the diffraction pattern is composed of a set of (primarily) non-overlapping diffraction spots. Examples of such data-sets are shown in Figs. 1 and 2. A large number of problems within polycrystal and powder research can be tailored to apply to this situation. In this case, the diffraction spots can be sorted with respect to element of origin, say the grain, by means of a polycrystalline indexing scheme (Lauridsen, Schmidt, Suter,

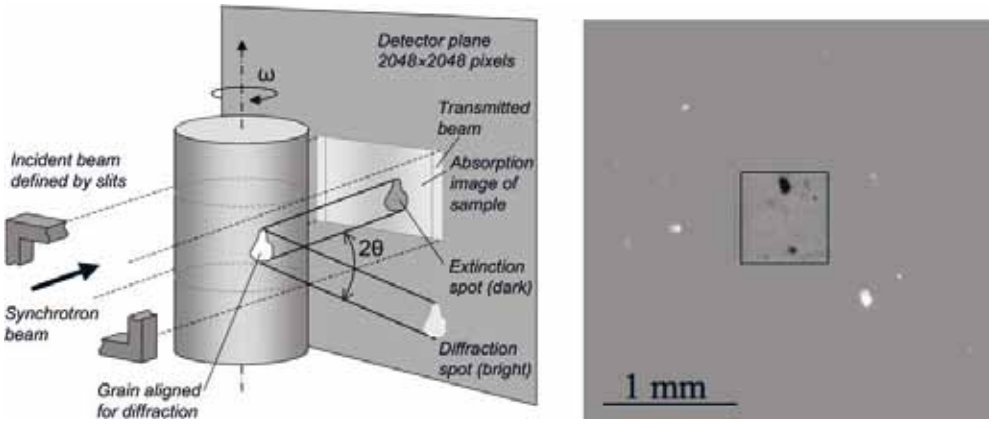


Fig 2. Left: DCT set-up. Grains in the sample can give rise to both conventional diffraction spots (dark-field image) and extinction spots (bright-field image). Adapted from Johnson, King, Honnicke, Marrow, and Ludwig (2008) Right: Example of a raw image acquired with this set-up. Diffraction spots are white and extinction spots are black. The box is the border of the direct beam. The sample is an annealed beta Ti polycrystal with grains of average size of 70 μm. The X-ray energy was 40 keV.

and Poulsen 2001). Several indexing programs exist: Grainspotter by S. Schmidt operates mainly on farfield data, and enables very fast data processing (S. Schmidt, in preparation). On the other hand, the DCT set-up uses a program based on near-field data and takes advantage of the use of Friedel pairs (Ludwig, Reischig, King, Herbig, Lauridsen, Johnson, Marrow, and Buffiere 2009).

The main limitation of any indexing program is in terms of the probability of spot overlap on the detector. The probability is determined by the number of grains, the texture, and the orientation spread of each grain. Simulations show that for samples with a weak texture and grains with a near-perfect lattice – that is with an orientation spread of the order 0.1 degree or less – one thousand grains can be indexed simultaneously. On the other hand, plastic deformation introduces orientation spread within the grains, which in practice prohibits indexing of embedded grains in materials that are deformed to more than 20%. A suggestion for an approach that extends indexing to larger degrees of spot overlap is provided by Hansen, Sørensen, Sükösd and Poulsen (2009).

Once a grain has been indexed all the tools of conventional single crystal diffraction analysis are available. Hence, a comprehensive characterisation of each grain immediately follows. If only the far-field detector is used the grain volume and average orientation can be characterised. Furthermore, one can determine the average values of all the components of the elastic strain tensor for each grain. The time resolution is often ~10 seconds, limited by the read-out time of the detector. The accuracy reported is in the best cases of order 0.1 deg for orientations and $\Delta\varepsilon/\varepsilon = 10^{-4}$ for the strain (see below). Furthermore, it is possible to perform a full crystallographic analysis of each grain; that is a structural refinement (Vaughan, Schmidt, and Poulsen 2004). The latter is relevant for instance for non-stoichiometric materials. If one or more high-spatial-resolution detectors are added to the set-up one can also determine the centre-of-mass position of each grain. However, this advantage is at the expense of time resolution, as the near-field detectors are much less efficient. To determine positions with high accuracy, a non-linear least square fit to the centre-of-mass (CMS) positions of the spots on the detector is performed. The accuracy at ID11 prior to the instalment of the 3D detector was ~3 μm.

As an example of center-of-mass mapping, we present results from a study of an undeformed IF steel sample. This was characterized layer-by-layer, covering 100 layers with a spacing of 10 μm. The 14121 2D grains found in these slices are superposed in Fig 3A. The snake-like appearance of the grains is due to different cross-sections having different centre-of-masses. Merging the appearance in successive layers, a map with 1843 three-dimensional grains is produced, cf Fig 3B. Further information about the experiment and a qualitative analysis of the observed lattice rotations after tensile deformation can be found in (Oddershede, Wright, Margulies, Huang, Poulsen, Schmidt and Winther 2010).

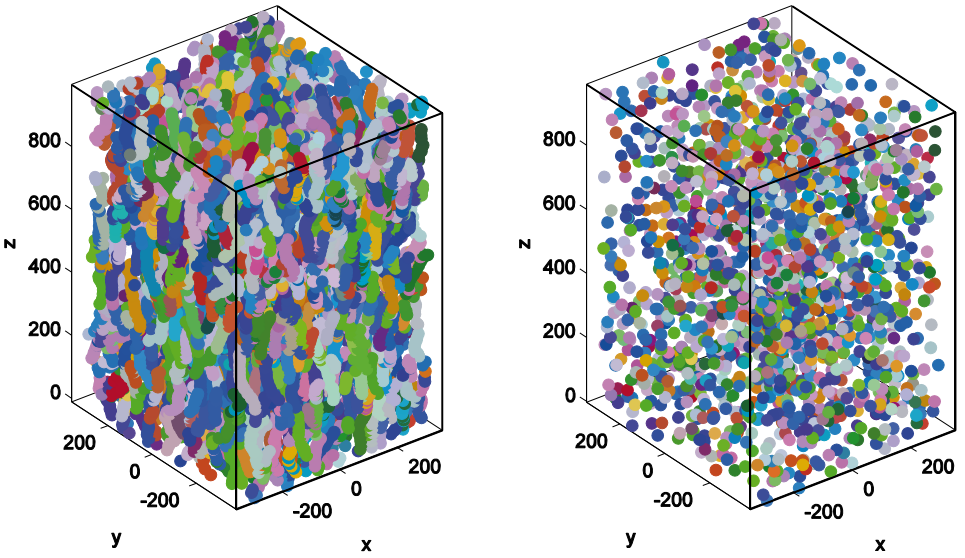


Fig. 3. Center-of-mass mapping of an undeformed IF steel specimen. The units on the axes are μm and the color coding is according to orientation. Left) Superposition of two-dimensional grains mapped layer-by-layer with a planar beam, and Right) Merging of 2D grains to three-dimensional grains, appearing in a minimum of two subsequent layers.

For very fast data acquisitions, one may simply repeat acquisitions with the far-field detector, oscillating within a narrow interval around a given ω–setting. Indexing is not possible in this case, but assuming grains do not rotate, one can monitor the change in volume of the grains giving rise to diffraction spots at this ω setting. Several hundred so-called *growth curves* of deeply embedded grains can be obtained simultaneously in this way (Lauridsen, Poulsen, Nielsen, and Juul Jensen 2003). Likewise this can be a fast way to characterize nucleation events.

3.1 Application: Nucleation and growth studies Traditionally, nucleation and growth phenomena have been analyzed using ensemble average properties, such as the volume fraction of transformed material. However, the predictive power of average properties is limited by the neglect of heterogeneities. For example, nucleation may take place preferentially at specific sites, and the growth rate of nuclei may depend strongly on orientation, size, stoichiometry, or relationships with neighbouring volumes. 3DXRD is an ideal tool to study the effect of heterogeneities, and as such it has been used for a series of studies related to recrystallization (Lauridsen *et al.* 2003), solidification (Iqbal**,** van Dijk, Offerman, Moret, Katgerman, and

Kearley 2005; Faraji, Wright, and Katgerman, 2010), and phase transformations in steel (Offerman, van Dijk, Sietsma, Grigull, Lauridsen, Margulies, Poulsen, Rekveldt, and van der Zwaag 2002), ceramics and ferro-electrics. In all cases it was demonstrated that the ensemble average "Avrami-type" models are at best gross simplifications. A recent application is the paper in these proceedings on the recrystallization kinetics of 50% cold rolled Aluminium (Poulsen, Lyckegaard, Oddershede, Lauridsen, Gundlach, Curfs, and Juul Jensen 2010).

3.2 Application: Elastic Strain mapping Determining the strain in individual grains is of interest in itself, e.g. for determining statistics of type-II stresses as input for plasticity models. Moreover, it is relevant for engineering, namely for characterising local stresses around cracks or defects, as the number of grains close to such objects often is too few for strain characterisation based on X-ray powder diffraction. Historically, the 3DXRD investigations have ranged from the first feasibility studies (Poulsen, Nielsen, Lauridsen, Schmidt, Suter, Lienert, Margulies, Lorentzen and Juul Jensen 2001; Margulies, Lorentzen, Poulsen and Leffers 2002; Martins, Margulies, Schmidt, Poulsen and Leffers 2004), over multiaxial stress states and resolved shear stresses in Ti (Reischig 2008) and in a Mg parent/twin cluster (Aydiner, Bernier, Clausen, Lienert, Tomé and Brown 2009) and selected grains in two Ti-7Al specimens (Lienert, Brandes, Bernier, Weiss, Shastri, Mills and Miller 2009), to the study of load partitioning in eight austenite and seven ferrite bulk grains in a two-phase duplex stainless steel (Hedström, Han, Lienert, Almer and Odén 2010). A step towards mapping stress fields of representative volumes was made when the grain resolved strains in 96 simultaneously illuminated grains of IF steel were followed during *in situ* tensile loading and unloading in the elastic regime (Oddershede, Schmidt, Poulsen, Sørensen, Wright and Reimers 2010). More recently, the grain resolved strains in more than 1000 grains within a copper specimen were followed from the undeformed state through the elasto-plastic transition (Oddershede, Schmidt, Poulsen and Reimers 2010).

3.3. Application: Grain rotations Polycrystalline deformation is a topic of prime interest to both metallurgists and geoscientists. However, despite 70 years of effort, there is no consensus on how to approach the modelling. In particular, it is unclear to what extent deformation behaviour is determined by the initial grain orientation, the grain-grain interactions or by the emerging dislocation structures. 3DXRD provides *in situ* methods for addressing these issues, for example through real-time observations of grain rotations in bulk materials during the deformation process (Margulies, Winther, and Poulsen, 2001). As an example the rotation path of 95 grains in a 4-mm-thick polycrystalline Al sample was determined during in situ tension to an elongation of 6% (Winther, Margulies, Schmidt, and Poulsen 2004). Such data provide a detailed combinatorial database for critical evaluation of models for polycrystalline deformation.

3.4. Application: Reciprocal space mapping of grains It is well known that the profiles of the peaks from single crystals comprise a wealth of information about defect densities, strain and domain sizes. Provided spot overlap is minimal, the approach presented above is well adapted to generalise such methods to studies of polycrystals. In the language of X-ray physics we may describe this as reciprocal space mapping of the individual grains. Typically, one requires a better angular (and thereby reciprocal space) resolution than provided by the standard far-field detector, placed at a distance of 20-40 cm. Hence, the three permanent 3DXRD microscopes all have the option of placing a detector at a distance of a few meters from the sample – not shown in Fig 1. This detector only captures a small fraction of the entire far-field pattern, sufficient to characterise the broadening of a single reflection.

Ungar and collaborators have used such a detector at ID11 to characterise Burgers vector populations, dislocation types and dislocation densities within individual grains of a

polycrystalline commercial-purity titanium specimen. The results provided can be used as input for different crystal-plasticity calculations and for the experimental verification of numerical simulations. (Ungar, Ribarik, Balogh, Salem, Semiatin, and Vaughan 2010).

At APS the options for reciprocal space mapping of grains has been further improved by the use of an x-ray monochromator with very low divergence and energy bandwidth (Lienert *et al.* 2010). In this so-called high angular resolution 3DXRD set-up, at 50 keV the longitudinal resolution in reciprocal space is as favourable as 1.7 $10^{-3}$ $Å^{-1}$.

One of the main applications of this set-up has been for studies of dislocation structures in fcc metals (Jakobsen, Poulsen, Lienert, Almer, Shastri, Sørensen, Gundlach and Pantleon, 2006). As an example a reciprocal space map of a grain within a Cu specimen is given in Fig 4. Notably, a direct space map of the dislocation structures is not provided in this way, but the peaks seen in Fig 4 can be correlated with individual sub-grains, and by characterising the widths and integral intensities of these peaks, one may determine the size, orientation and strain components of the corresponding individual sub-grains. One of the findings is that there is a heterogeneous distribution of internal stresses between sub-grains (Jakobsen, Poulsen, Lienert and Pantleon 2007). This discovery requested a reformulation of the standard composite model. Similar results have been obtained with spatially resolved observations using differential-aperture X-ray microscopy (Levine, Larson, Yang, Kassner, Tischler, Delos-Reyes, Fields and Liu 2006; Levine, Larson, Tischler, Geantil, Kassner, Liu, and Stout 2008).

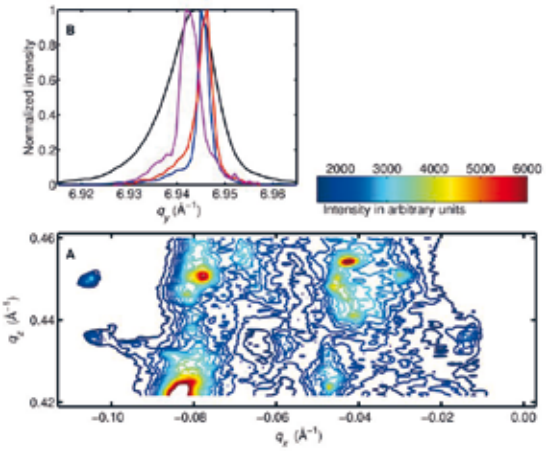


Fig 4. A reciprocal map for one (400) reflection from one deeply embedded grain within a 300 μm thick Cu tensile specimen at 3.49% elongation. (A) Projection onto the azimuthal plan of the full ($q_x$, $q_y$, $q_z$) reciprocal space intensity map. The map is truncated in $\mathbf{q}_z$. The color scale is above the map. (B) Strain profiles of a few of the peaks appearing in the map; that is the intensity distribution projected on $\mathbf{q}_y$ (red, blue, magenta). The corresponding profile for the entire map is indicated in black. From Jakobsen *et al.* (2006).

The real power of the technique however is for *in situ* studies of the formation and refinement of sub-grains. Initially, a longstanding discussion was settled by proving that dislocations assemble in boundaries already during the deformation and from the on-set of plasticity (Pantleon, Wejdemann, Jakobsen, Lienert and Poulsen 2009). Next, significant changes in the distribution of internal stresses during stress relaxation and unloading were observed (Jakobsen, Poulsen,

Lienert, Bernier, Gundlach and Pantleon 2009). Recently focus has been strain path changes, where pre-deformed specimens are tensile deformed in a new direction while monitoring the evolution of the dislocation structures, see Pantleon, Wejdemann, Jakobsen, Lienert and Poulsen (2010) in these proceedings.

## 4. VOLUMETRIC MAPPING

The reconstruction techniques presented in this section aim at rendering 3D grain morphologies and more generally at providing a voxel-by-voxel map of the local orientation. The development of such algorithms is non-trivial, as the complexity in terms of the dimensionality and sheer size of the reconstruction space is much larger than *e.g.* for absorption contrast tomography. Another difference is that in 3DXRD the number of useful projections is given by the number of observable reflections, which may be limited by experimental geometry to be as few as five. A number of alternative algorithmic approaches have been developed to overcome these issues. In the following we make a brief distinction between approaches and present a number of recent results, demonstrating the status of the techniques:

4.1 Indexing and grain-by-grain reconstruction In this approach one relies on an indexing algorithm to initially identify a set of diffraction spots for each grain. Based on the intensity distribution of these spots, the 3D maps of the grains are reconstructed independently (Fu, Poulsen, Schmidt, Nielsen, Lauridsen and Juul Jensen, 2003). The individual grain maps are then superposed. The result may be a map of the sample with minor overlaps and voids between grains – these are resolved *e.g.* by applying morphological operators or using Gibbs priors (Alpers, Poulsen, Knudsen and Herman, 2006).

The software associated with the *DCT set-up* is currently based on this approach. The actual reconstruction of each grain is made by the Algebraic Reconstruction Technique (ART). Typically ω-steps of 0.1 degrees and an ω-range of 360 degrees are used, which, depending on beamline and optics, imply that the acquisition of a full 3D map takes between 0.1 and 10 hours. Maps with 1000+ grains are now made routinely, with a spatial resolution of 2-3 μm. As an example we mention the work on stress corrosion cracking in an austenitic stainless steel sample (King, Johnson, Engelberg, Ludwig, and Marrow 2008). Here tomography was used to monitor *in situ* the evolution of the crack in 3D, which was then correlated to the 3D grain structure. Several sensitization-resistant crack-bridging boundaries were identified, which were not the twin variant boundaries usually maximized during grain boundary engineering. For other application examples see (Ludwig, King, Reischig, Herbig, Lauridsen, Schmidt, Proudhon, Forest, Cloetens, Roscoat, Buffiere, Marrow, and Poulsen 2009; King, Herbig, Ludwig, Reischig, Lauridsen, Marrow, and Buffiere 2009; Syha, Baurer, Hoffmann, Lauridsen, Ludwig, Weygand, and Gumbsch 2010).

The spatial resolution of volumetric mapping techiques presented in this section is determined by the X-ray detector. With the DCT set-up it is possible – at the expense of the detector being very close to the sample - to go to the limit of the existing detector technology by using very high magnification optics within the camera. To demonstrate this, in Fig 5 we present a recent study made at beamline ID19, ESRF of a 4N-Al wire. The sample material was originally ARB-processed to a strain of 4.8, which subsequently had been annealed at 175 $^{o}$C for 6 h and 250 $^{o}$C for 30 minutes. The resulting microstructure exhibits a low fraction of low-angle boundaries and an average grain size of 3.9 μm (Kamikawa, N., Tsuji, N., Huang, X., and Hansen, N. 2006). The set-up involved an X-ray energy of 17.6 keV, a double-Bragg Si(111) monochromator, a sample-to-fluorescence-screen distance of 0.58 mm and an optical magnification of 60, resulting

in a pixel size of 225 nm. The exposure time was 9 s per image. The resulting spatial resolution in 3D is estimated to be 500 nm.

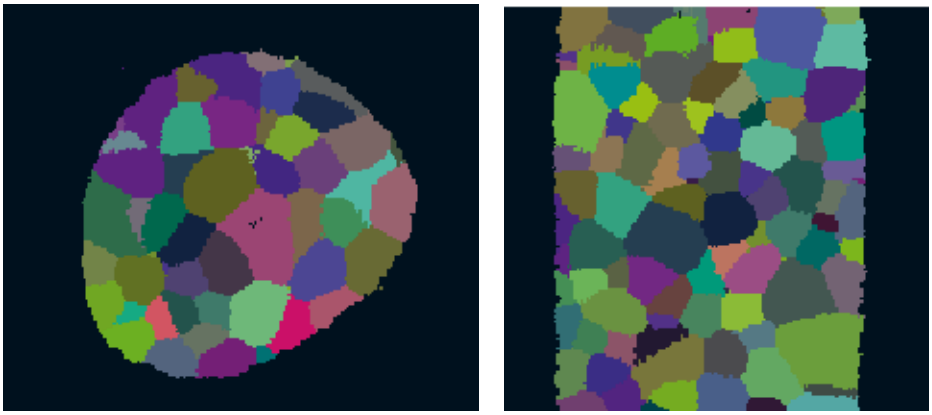

Fig 5. 3D map of the grains within an annealed Al wire. Left: transverse cross-section, right: longitudinal cross-section. The pixel size is 225 nm and the diameter of the wire is on average 20 μm. The colours denote orientations. Work by Reischig, Lauridsen, Poulsen and Ludwig.

The methods presented above are based on the critical assumption that the grains are "undeformed"; that is that orientation gradients within the grains either are absent or small in comparison to the size of the ω–step. Experience has shown that even for recrystallised metals, this is often not the case, as an orientation spread of 0.1-1 degree may be present. To overcome this issue, it is relevant to generalise the methodology to include the possibility of such gradients within each grain.

In Rodek, Poulsen, Knudsen, and Herman, (2007) a Monte-Carlo algorithm is suggested for handling this task – however, it was only tested by simulations. In the article by King, Reischig, Martin, Fonseca, Preuss, and Ludwig (2010) elsewhere in these proceedings two other algorithms are explored for obtaining information on the sub-grain scale. One of these is based on inserting a regular grid between the sample and the detector. Preliminary results of a study on polycrystalline Al are also included.

4.2 Topo-tomography This is an alternative procedure, which allows reconstructing a single grain, using a set-up with additional tilt-stages (Ludwig, Lauridsen, Schmidt, Poulsen, and Baruchel 2007). For a selected grain, the scattering vector of a suited reflection is aligned parallel to the rotation axis of the tomographic setup. This particular setting assures that the diffraction condition is maintained while the sample is turned 360° around the rotation axis. In this case the grain reconstruction can be performed from data acquired in direct and/or in diffracted beam by means of a standard (cone beam) filtered backprojection algorithm. In comparison to reconstructions by 3DXRD above, the spatial resolution are often substantially better since a large number of equally spaced reflections can be acquired on a detector screen adjusted to the grain size, but are ultimately limited by current detector technology. The disadvantage is the restriction to one grain only.

4.3 Orientation Imaging Microscopy Orientation Imaging microscopy (OIM) is well known from electron microscopy, where a scanning method – Electron Backscatter Diffraction (EBSD) – is used to create maps of the orientations in a layer point-by-point. The 3DXRD equivalent is a 3D map, where the orientation in each voxel of the sample is reconstructed independently. Grains and grain boundaries are then defined in a post-processing step, similar to EBSD software. In comparison to the grain-by-grain reconstruction case presented in section 4.1 this approach has the advantage that a space-filling map is automatically generated. The drawback is that mathematically speaking the solution space is much enlarged, implying that the reconstruction will be slower.

The workhorse for ID11 has been the program *Grainsweeper* by S. Schmidt. This may operate on data arising from one or more screens, such as those shown in Fig 1. This program produced the first grain map on a statistically relevant number of grains: 483, as part of a study of grain growth in Al-0.1% Mn (Schmidt, Olsen, Poulsen, Sørensen, Lauridsen, Margulies, Maurice, and Juul Jensen, 2008). Maps of 1000+ grains are now made routinely. The sample diameter is typically in the range 0.5-1 mm, while the spatial resolution until the recent installation of the 3D detector was limited by the detector point-spread-function to 5 μm.

A main focus point has been to map individual bulk grains and directly watch their growth *in-situ* during recrystallization of deformed metals. A number of combinations of the orientation of the new grain and the orientation of the deformed matrix have been investigated; see e.g. Schmidt, Nielsen, Gundlach, Margulies, Huang, and Juul Jensen (2004). In all cases, it was found that the growth was much more complex than hitherto anticipated. The observations show that the growth is highly heterogeneous (even in very homogeneous deformed microstructures), the growth rates vary in space and time, it is jerky in the sense that a given boundary segment may move then stop for a while and then move forward again and locally protrusions form on the migrating boundary. The most recent experiments however were performed by topo-tomography (Van Boxel, Schmidt, Ludwig, Zhang, Sørensen, Pantleon, and Juul Jensen 2010) in an attempt to increase the spatial resolution.

The workhorse for the studies at beamline 1-ID is the *Monte Carlo optimisation software* by Suter and collaborators (Suter, Hennessy, Xiao and Lienert 2006). This software has been tested in detail based on both simulations and experimental data. As an example we mention work on high purity, well annealed nickel (Hefferan, Li, Lind, Lienert, Rollett, Wynblatt, and Suter 2009). In this case statistics on grain orientations, intra-granular misorientations, and nearest neighbor grain misorientations were compared to statistics from EBSD. The correspondence was satisfactory, and it was furthermore demonstrated that the orientation resolution with the set-up at 1-ID is better than 0.1 degree. Extensive 3D maps of this kind have been generated with a spatial resolution of 5 microns. Some examples are provided in these proceedings (Lienert *et al*. 2010).

The examples mentioned above relate to (nominally) undeformed samples. However, a main motivation for introducing the orientation imaging algorithms is to be able to map moderately or even heavily deformed materials, where the diffractions spots from the individual grains will overlay substantially. It is not trivial that such maps can be generated by 3DXRD, as each voxel in a deformed specimen may be associated with several orientations (several sub-grains) or even an orientation distribution, and the diffraction patterns observed are a superposition of contributions from such distributions for all illuminated voxels. However, encouraging results have been obtained from simulations, indicating that convergence is possible for at least 20-30% tensile deformation (Rodek *et al.* 2007; Lienert *et al.* 2010).

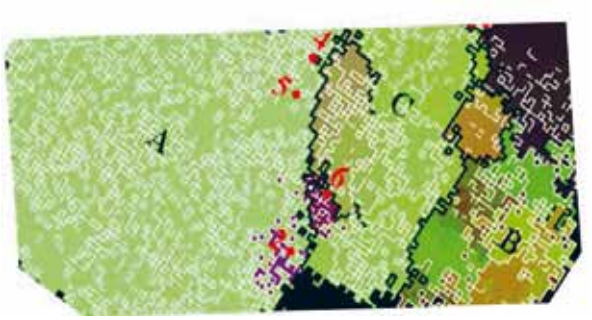


Fig 6. 3DXRD based OIM map of one layer within a 30% cold-rolled Al1050 sample. The colors indicate orientations, white and black lines mis-orientations of 2 and 15 degrees, respectively. Three grains are identified and marked as A, B and C. Superposed on the OIM map is the position of four nuclei found to appear in or near to this layer during subsequent annealing (red dots). The longer dimension of the cross-section is 1000 μm. From West *et al.* (2009).

First experimental data - for a 30% cold-rolled Al sample - are presented in West, Schmidt, Sørensen, Winther, Poulsen, Margulies, Gundlach, and Juul Jensen (2009). A reconstructed map from one of the 100 layers investigated is reproduced here as Fig 6. The spatial resolution of this map is estimated to be 30 μm, and the statistical noise on orientations is of order 2 degrees. For most purposes these values are insufficient. However, it should be emphasized that the map in this particular case was based on data acquired with a low spatial resolution detector: the FReLoN camera (Labiche, Mathon, Pascarelli, Newton, Guilera, Curfs, Vaughan, Homs, and Carreiras, 2007). This detector has a pixel size of 50 μm and as such the data comprise very limited spatial information. The fact that a map could be generated with such a detector is again encouraging.

The strategy at ID11 is in the future to base 3D OIM maps on data acquired at all three distances, cf. Fig 1. Simulations point to a resolution of a few microns in this case. First experiments with the new 3D detector have been performed by S. Schmidt and co-workers, and the analysis is ongoing.

Ludwig and co-workers currently explore the possibilities of an optimized 3DXRD line beam acquisition geometry with an additional near field detector at scattering angles close to 90 degrees. Although limited to X-ray energies below 20 keV, this approach bears potential for substantial improvement of spatial as well as orientation and strain resolution (Ludwig, King, Herbig, Reischig, Proudhon, and Buffiere 2010).

We end by emphasizing that both the Grainsweeper and the Monte-Carlo optimization programs are based on layer-by-layer reconstructions. Evidently, the data acquisition would be faster, if a more extensive part of the sample was illuminated. To what extent 3DXRD OIM mapping is feasible in this mode for deformed specimens is an open question.

## 5. BOX-SCAN TECHNIQUE

Characterisation of large sample volumes is complicated by the spot overlap issue as well as by the fact that it may not be possible to condition the monochromatic beam to illuminate the whole volume at once. For such cases it is relevant to develop approaches, where the volume of

interest is divided into a set of sub-volumes, to be characterised successively (Poulsen 2004). Another general concern is that the use of a near-field detector is prohibitive for certain *in situ* studies, which involve large samples or spacious sample surroundings.

The so-called "box-scan technique" addresses these shortcomings (Lyckegaard, Poulsen, Ludwig, Fonda, Margulies, Gotz, Sørensen, Dey and Lauridsen 2010). The set-up involves a far-field detector only, and is therefore applicable also to work on coarse-grained specimens with laboratory X-ray systems. The box refers to the part of the specimen to be investigated. For plate-like specimens, this will be a volume of dimensions V x H x T, where V and H relate to vertical and horizontal dimensions and T is the thickness of the specimen. The procedure is as follows

1) First a horizontal "line-beam" is used: by focusing and/or the use of slits the incoming beam is confined to dimensions V1 x H1, where V1 << V and H1 is somewhat larger than H. The sample is translated successively in the vertical direction (z) over the range of V and in steps of V1, and for each of these steps a regular 3DXRD $\omega$-scan is made. By thresholding the images, this procedure leads to the identification of a set of diffraction spots, characterised by their centre-of-mass z- , $\omega$- and $\eta$-positions ($\eta$ is the azimuthal angle, defined in fig 1). The (x,y) position of the corresponding grains are at this point unknown.

2) Next a vertical "line-beam" is used: by focusing and/or the use of slits the incoming beam is confined to dimensions V x H2, where H2 << H. The sample is translated successively in the horizontal direction over a range of H1 and in steps of H2, and for each of these steps a regular 3DXRD $\omega$-scan is made. By thresholding the images, this procedure leads to the identification of a set of spots, characterised by their centre-of-mass $\omega$- and $\eta$-positions. In addition for each spot we know that the centre of the associated grain is positioned along a certain line in the (x,y) plane of the sample.

3) The box-scan algorithm identifies which spots are the same in the two types of scan and uses the combined information as input for indexing. The result is a grain centre map. Similar to what was reported in section 3, for each grain the position, orientation and size is deduced. Strain would also be an option but has not been implemented.

Notably, the number of data acquisitions required with this approach is ~2N*M, where N is the average number of translational steps in one of the two sessions and M is the number of $\omega$-settings. In contrast, a true point-to-point 3D scanning procedure with a monochromatic beam would require ~$N^3$*M acquisitions. Typical values for characterisation of a volume of say H = V = T = 0.5 mm could be V1 = H2 = 5 $\mu$m, H1 = 0.7 mm, an $\omega$-range of 120 degrees and an $\omega$-step of 0.5 deg. Hence, N = 100, M = 240, and the total number of acquisitions for the box-scan and the 3D scanning procedure becomes 48,000 and 240,000,000, respectively. These numbers demonstrate the relevance of the approach.

The box-scan algorithm has been validated by a study of $\beta$21-Ti with an average grain size of 30 $\mu$m. For this particular material, the resulting 3D grain map could be compared directly to a grain map generated by X-ray tomography (with a resolution of 1 $\mu$m). The quality of the data is illustrated in Fig 7, where the tomography and box scan data are compared for one layer of the sample. Out of the 159 grains found by tomography to be partially or fully within the volume-of-interest – "the box" – 23 were missing in the box-scan results. However, except for 3 these were at the boundaries of the box (and therefore not fully illuminated) or were very small. On

top the box-scan algorithm generated 4 false positives. Encouragingly the average error on grain positions was 2.6 μm, substantially less than the step-size of 5 μm used.

The first applications of the technique, generating 3D grain centre maps of 1000+ grains, have recently been produced at beamline 1-ID. This work by Miller and co-workers will be presented elsewhere.

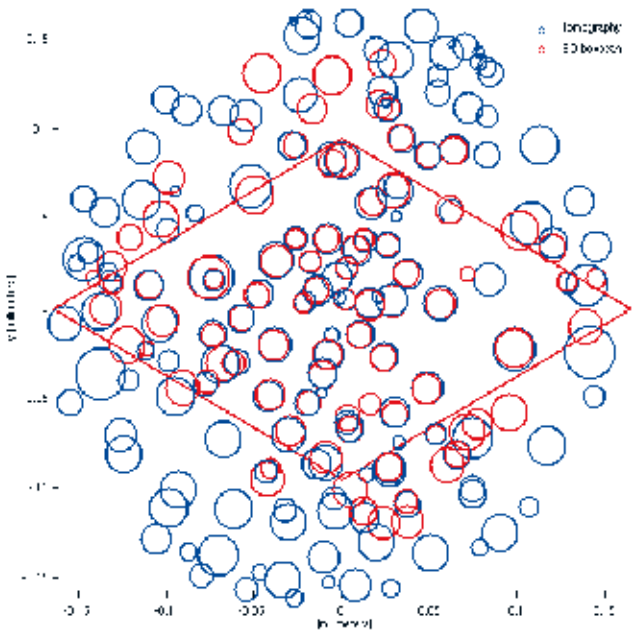

Fig 7. Validation of the box-scan algorithm on a cylindrical sample of β-Ti. Shown is one cross-section of the sample, which has a diameter of 300 μm. Red circles mark the centre position and size of the grains as determined by the box scan approach. Blue circles mark the corresponding results from a reference reconstruction based on X-ray tomography. The box-shaped area confined by red lines is the area-of-interest for the box-scan approach.

5.1 Laguerre tessellation: a route to voxelated maps from grain centre maps. It is of interest to be able to convert the grain center maps discussed above and in section 3 to approximate voxelated maps for use as input to Finite Element Modeling, phase field modeling or similar. In Lyckegaard, Lauridsen, Ludwig, Fonda, and Poulsen (2010) it is suggested that the combined information of position and volume of the grains is used as input for a Laguerre tessellation scheme. The quality of the resulting maps was determined in another experimental study of β-Ti. Shown in Fig 8 is a superposition of the results of the tessellation and the "true" grain map, as revealed by tomography. On average 14% of the voxels are assigned to the wrong grain, and each grain has 1.4 false neighbors. In our opinion this quality is sufficient for a range of modeling efforts.

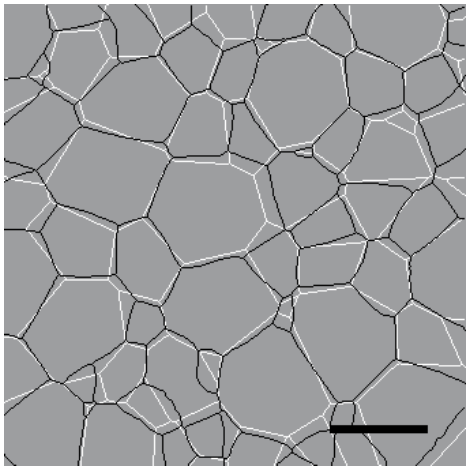

Figure 8: Experimental study of the quality of Laguerre tessellations based on knowledge of the positions and volume of the grains. Shown is one layer within a 3D□-Ti sample. The white lines represent the results of the tessellation while the black lines represent the real microstructure. The scale bar is 50 □m. From Lyckegaard *et al.* (2010).

Notably, within the box-scan approach, additional information on the morphology of the grains is available. By plotting the intensity of the spots as function of translation one can derive e.g. the moment-of-inertia or the aspect ratio of the associated grains. (Similarly, in the layer-by-layer mode illustrated in Fig 3A, additional information is available from the snake-like appearance of each grain.) It is an interesting question to what extent this additional information can improve the quality of the grain maps and how many additional projections are required to produce maps of the same quality as the volumetric ones based on the use of a near-field detector. A first attempt at addressing these questions can be found in these proceedings (Lyckegaard, Alpers, Ludwig, Fonda, Margulies, Götz, Sørensen, Dey, Poulsen, and Lauridsen, 2010).

## ACKNOWLEDGEMENTS

The authors gratefully acknowledge the Danish National Research Foundation for supporting the Centre for Fundamental Research: Metal Structures in Four Dimensions, within which this work was performed. The Danish Research Council is acknowledged for funding the synchrotron experiment (via Danscatt), while J.O. acknowledges funding from the German Bundesmini-sterium für Bildung und Forschung. ESRF is thanked for beamtime.

## REFERENCES

Alpers, A., Poulsen, H.F., Knudsen, E., and Herman, G.T. (2006). A discrete tomography algorithm for improving the quality of three-dimensional X-ray diffraction grain maps. J. Appl. Cryst. 39, 582-588

Aydiner, C.C., Bernier, J.V., Clausen, B., Lienert, U., Tomé, C.N. and Brown, D.W. (2009). Evolution of stress in individual grains and twins in a magnesium alloy aggregate. Physical Review B, 80, 024113.

Barabash, R.I., Tischler, J., Ice, G.E., and Barabash, O.M. (2010). Small scale mechanical behaviour and interface strength in Ni-Mo Composites from 3D X-ray microdiffraction, *in* N. Hansen *et. al* (ed.). Proceedings *of the 31st. Risø International Symposium on Materials Science, Risø National Laboratory, Roskilde, Denmark*

Bleuet, P., Welcomme, E., Dooryhee, E., Susini, J., Hodeau, J.L., and Walter, P (2008). Probing the structure of heterogeneous diluted materials by diffraction tomography. Nature Mater. 7, 468-472

Bunge, H.J., Wcislak, L., Klein, H., Garbe, U, and Schneider, J.R. (2003). Texture and microstructure imaging in six-dimensions with high-energy synchrotron radiation. J. Appl. Cryst. 36, 1240-1255

Faraji, M. Wright, J.P., and Katgerman, L. (2010). In-situ observation of the nucleation kinetics and the mechanism of grain refinement in Al–Si alloys (Part I) Materials Letters 64, 1016–1018

Fu, X., Poulsen, H.F., Schmidt, S., Nielsen, S.F., Lauridsen, E.M., and Juul Jensen, D. (2003). Non-destructive mapping of grains in three dimensions. Scripta Mater. 49,1093-1096

Hansen, P.C., Sørensen, H.O., Sükösd, Z., and Poulsen, H.F. (2009). Reconstruction of single-grain orientation distribution functions for crystalline materials. SIAM Journal of Imaging Sciences 2, 593-613

Hedström, P., Han, T.-S., Lienert, U., Almer, J. and Odén, M. (2010). Load partitioning between single bulk grains in a two-phase duplex stainless steel during tensile loading. Acta Materialia, 58, 734-744.

Hefferan, C.M., Li, S.F., Lind, J., Lienert, U., Rollett, A.D., Wynblatt, P., and Suter R.M. (2009). Statistics of high purity nickel microstructure from high energy X-ray diffraction microscopy. Computers, Materials and Continua, 14, 209-219.

Ice, G.E., Larson, B.C., Yang, W., Budai, J.D., Tischler, J.Z., Pang, J.W.L., Barabash, R.I, and Liu, W. (2005). Polychromatic X-ray microdiffraction studies of mesoscale structure and dynamics J. Synchrotron Rad. 12, 155-162

Ice, G.E. and Pang, J.W.L. (2010). Polychromatic microdiffraction studies of 3D elastic and plastic strain tensors *in* N. Hansen *et. al* (ed.). Proceedings *of the 31st. Risø International Symposium on Materials Science, Risø National Laboratory, Roskilde, Denmark*

Iqbal**,** N., van Dijk, N.H., Offerman, S.E., Moret, M.P., Katgerman, L. and Kearley G.J. (2005), Real-time observation of grain nucleation and growth during solidification of aluminium alloys, Acta Mater. 53, 2875-2880.

Jakobsen, B., Poulsen, H.F., Lienert, U., Almer, J., Shastri, S.D., Sørensen, H.O., Gundlach, C., and Pantleon, W. (2006). Formation and subdivision of deformation structures during plastic deformation, Science 312, 889-892.

Jakobsen, B., Poulsen, H.F., Lienert, U., and Pantleon W. (2007). Direct determination of elastic strains and dislocation densities in individual subgrains in deformation structures, Acta mater. 55, 3421-3430.

Jakobsen, B., Poulsen, H.F., Lienert, U., Bernier, J., Gundlach, C., and Pantleon W. (2009). Stability of dislocation structures in copper towards stress relaxation investigated by high angular resolution 3D X-ray diffraction, phys. stat. sol. 206, 21-30.

Johnson, G., King, A., Honnicke, M.G., Marrow, J., and Ludwig, W. (2008). X-ray diffraction contrast tomography: a novel technique for three-dimensional grain mapping of Polycrystals. II. The combined case. J. Appl. Cryst. 41, 310-318.

Kamikawa, N., Tsuji, N., Huang, X., and Hansen, N. (2006). Quantification of annealed microstructures in ARB processed aluminum Acta Materialia 54, 3055-306

King, A., Johnson, G., Engelberg, D., Ludwig, W., and Marrow, J. (2008). Observations of intergranular stress corrosion cracking in a grain-mapped poylcrystal. Science 321, 382–385

King, K., Herbig, M., Ludwig, W., Reischig, P., Lauridsen, E.M., Marrow, J., and Buffiere, J. (2009). Non-destructive analysis of micro texture and grain boundary character from X-ray diffraction contrast tomography. Nuclear Inst. and Methods in Physics Research, B, 268, 291–296.

King, A., Reischig, P., Martin, S., Fonseca, J., Preuss, M., and Ludwig, W. (2010). Grain mapping by diffraction contrast tomography: extending the technique to sub-grain information, *in* N. Hansen *et. al* (ed.). Proceedings *of the 31st. Risø International Symposium on Materials Science, Risø National Laboratory, Roskilde, Denmark*

Labiche J.-C., Mathon, O., Pascarelli, S., Newton, M., Guilera, G., Curfs, C., Vaughan, G., Homs, A., and Carreiras, D.F. (2007). The fast readout low noise camera as a versatile X-ray detector for time resolved dispersive extended X-ray absorption fine structure and diffraction studies of dynamic problems in materials science, chemistry, and catalysis. Rev. Sci. Instrum 78, 091301.

Larson, B.C. , Yang, W., Ice, G.E., Budai, J.D. and Tischler, T.Z. (2002). Three dimensional X -ray structural microscopy with submicrometre resolution. Nature 415, 887-890.

Lauridsen, E.M., Schmidt, S., Suter, R.M., and Poulsen, H.F. (2001). A method for structural characterization of grains in powders or polycrystals. J. Appl. Cryst. 34**,** 744-750

Lauridsen, E.M., Poulsen, H.F., Nielsen, S.F., and Juul Jensen, D. (2003). Recrystallization kinetics of individual bulk grains in 90 % cold-rolled aluminium. Acta Mater. 51, 4423-4435.

Levine, L. E., Larson, B. C., Yang, W., Kassner, M. E., Tischler, J. Z., Delos-Reyes, M. A., Fields, R. J., and Liu, W. (2006). X-ray microbeam measurements of individualdislocation cell elastic strains in deformed single-crystal copper. Nat. Mater. 5, 619-622.

Levine, L. E., Larson, B. C., Tischler, J. Z., Geantil, P., Kassner, M. E., Liu, W, and Stoudt, M. R. (2008). Impact of dislocation cell elastic strain variations on line profiles from deformed copper. Z. Kristallogr. Suppl. 27, 55-63.

Lienert, U., Brandes, M.C., Bernier, J.V., Weiss, J., Shastri, S.H., Mills, M.J. and Miller, M.P. (2009). In situ single-grain peak profile measurements on Ti-7Al during tensile deformation. Materials Science and Engineering A, 524, 46-54.

Lienert, U., Brandes, M.C., Bernier, J.V., Mills, M.J., Miller, M.P., Li, S.F., Hefferan, C.M., Lind, J., and Suter, R.M. (2010). 3DXRD at the Advanced Photon Source: orientation mapping and deformation studies *in* N. Hansen *et. al* (ed.). Proceedings *of the 31st. Risø International Symposium on Materials Science, Risø National Laboratory, Roskilde, Denmark*

Ludwig, W., Lauridsen, E.M., Schmidt, S., Poulsen, H.F., and Baruchel, J. (2007). High-resolution three-dimensional mapping of individual grains in polycrystals by topotomography. J. Appl. Cryst. 40 , 905-911

Ludwig, W. Reischig, P. King, A. Herbig, M. Lauridsen, E. M. Johnson, G. Marrow, T. J. and Buffiere, J. Y. (2009). Three-dimensional grain mapping by x-ray diffraction contrast tomography and the use of Friedel pairs in diffraction data analysis. Review of Scientific Instruments 80, 33905 - 33905-9

Ludwig, W., King, A., Reischig, P., Herbig, M., Lauridsen, E.M., Schmidt, S, Proudhon, H., Forest, S., Cloetens, P., d. Roscoat, S.R., Buffiere, J.Y., Marrow, T., and Poulsen, H.F. (2009). New opportunities for 3D materials science of polycrystalline materials at the micrometre lengthscale by combined use of X-ray diffraction and X-ray imaging. Materials Science and Engineering: A, 524, 69–76.

Ludwig, W., Reischig, P., King, A., Herbig, M., Proudhon, H., Buffiere, J.Y., Rutishauser, S.and David, C. (2010). Thoughts about the optimum data acquisition geometry and time resolution of monochromatic beam X-ray diffraction microscopy experiments, *in* N. Hansen *et. al* (ed.). Proceedings *of the 31st. Risø International Symposium on Materials Science, Risø National Laboratory, Roskilde, Denmark*

Lyckegaard, A., Lauridsen, E.M., Ludwig, W., Fonda, R., and Poulsen, H.F. (2010). On the use of Laguerre tessellations for presentations of 3D grain structures. Image Analysis Stereology, in print.

Lyckegaard, A., Alpers, A., Ludwig, W., Fonda, R.W., Margulies, L., Götz, A. Sørensen, H.O., Dey, S.R., Poulsen, H.F., and Lauridsen, E.M. (2010). 3D grain reconstruction from boxscan data, *in* N. Hansen *et. al* (ed.). Proceedings *of the 31st. Risø International Symposium on Materials Science, Risø National Laboratory, Roskilde, Denmark*

Lyckegaard, A., Poulsen, H.F., Ludwig, W., Fonda, R.W., Margulies, L., Gotz, A., Sørensen, H.O., Dey, S.R. and Lauridsen, E.M (2010). Boxscan: A novel 3DXRD-based method for mapping of polycrystalline materials. In preparation.

Margulies, L., Lorentzen, T., Poulsen, H.F. and Leffers, T. (2002). Strain tensor development in a single grain in the bulk of a polycrystal under loading. Acta Mater. 50, 1771-1779.

Margulies, L., Winther, G., and Poulsen, H.F. (2001), In situ measurement of grain rotation during deformation of polycrystals. Science 291, 2392-2394

Martins, R.V., Margulies, L., Schmidt, S., Poulsen, H.F. and Leffers, T. (2004). Simultaneous measurement of the strain tensor of 10 individual grains embedded in an Al tensile sample. Mater. Sci. Eng. A 387-389, 84-88.

Oddershede, J., Schmidt, S., Poulsen, H.F., Sørensen, H.O., Wright, J. and Reimers, W. (2010). Determining grain resolved stresses in polycrystalline materials using three-dimensional X-ray diffraction. J. Appl. Cryst. 43, 539-549.

Oddershede, J., Schmidt, S., Poulsen, H.F. and Reimers, W. (2010). Measuring Type II Stresses Using 3DXRD. Mater. Sci. Forum 652, 63-69.

Oddershede, J., Wright, J.P., Margulies, L., Huang, X., Poulsen, H.F., Schmidt, S. and Winther, G. (2010). 3DXRD measurements of lattice rotations in tensile deformed IF steel. Proceedings of the 31st Risø International Symposium on Materials Science.

Offerman, S.E. van Dijk, N.H., Sietsma, J., Grigull, S., Lauridsen, E.M., Margulies, L., Poulsen, H.F., Rekveldt, M.T, and van der Zwaag, S. (2002). Grain nucleation and growth during phase transformations. Science 298**,** 1003-1005.

Pantleon, W., Wejdemann, C., Jakobsen, B., Lienert, U., and Poulsen, H.F. (2009). Evolution of deformation structures under varying loading conditions followed in-situ by high angular resolution 3DRXD, Mater. Sci. Engng. A 524, 55-63.

Pantleon, W., Wejdemann, C., Jakobsen, B., Lienert, U., and Poulsen, H.F. (2010). Advances in characterization of deformation structures by high resolution reciprocal space mapping, *in* N. Hansen *et. al* (ed.). Proceedings *of the 31st. Risø International Symposium on Materials Science, Risø National Laboratory, Roskilde, Denmark*

Poulsen, H.F., Nielsen, S.F., Lauridsen, E.M., Schmidt, S., Suter, R.M., Lienert, U., Margulies, L., Lorentzen, T. and Juul Jensen, D. (2001). Three-dimensional maps of grain boundaries and the stress state of individual grains in polycrystals and powders. J. Appl. Cryst. 34, 751-756.

Poulsen, H.F. (2004). Three-dimensional x-ray diffraction microscopy (Springer, Berlin).

Poulsen, H.F. (2009). Three-dimensional x-ray diffraction. In: Advanced tomographic methods in materials research and engineering. Ed.: Banhart, J. (Oxford University Press. Oxford), 249-276.

Poulsen, S.O., Lyckegaard, A., Oddershede, J., Lauridsen, E.M., Gundlach, C., Curfs, C. and Juul Jensen, D. (2010). Recrystallization kinetics of 50% cold-rolled aluminium *in* N. Hansen *et. al* (ed.). Proceedings *of the 31st. Risø International Symposium on Materials Science, Risø National Laboratory, Roskilde, Denmark*

Reischig, P. (2008) Determination of elastic strain tensors from X-ray diffraction contrast tomography. Masters thesis, Delft University of Technology.

Rodek, L., Poulsen, H.F., Knudsen, E., and Herman, G.T. (2007). A stochastic algorithm for reconstruction of grain maps of moderately deformed specimens based on X-ray diffraction. J. Appl. Cryst. 40, 313-321

Schmidt, S., Nielsen, S.F., Gundlach, C., Margulies, L., Huang, X., and Juul Jensen, D. (2004). Watching the growth of bulk grains during recrystallization of deformed metals. Science 305, 229-232

Schmidt, S., Olsen, U.L., Poulsen, H.F., Sørensen, H.O., Lauridsen, E.M., Margulies, L., Maurice, C., and Juul Jensen, D. (2008), Direct observation of 3-D grain growth in Al-0.1% Mn. Scripta Mater. 59, 491-494

Suter, R.M., Hennessy, D., Xiao, C., and Linert, U. (2006). Forward modeling method for microstructure reconstruction using x-ray diffraction microscopy: single crystal verification. Rev. Sci. Instr. 77, 1-12.

Syha, M. Baurer, M., Hoffmann, M.J., Lauridsen, E.M., Ludwig, W., Weygand, D., and Gumbsch, P. (2010). Comparing grain growth experiments and simulations in 3D *in* N. Hansen *et. al* (ed.). Proceedings *of the 31st. Risø International Symposium on Materials Science, Risø National Laboratory, Roskilde, Denmark*

Ungar, T., Ribarik, G., Balogh, L., Salem, A.A., Semiatin, S.L., and Vaughan G.B.M. (2010). Burgers vector population, dislocation types and dislocation densities in single grains extracted from a polycrystalline commercial-purity Ti specimen by X-ray line-profile analysis. Scripta Materialia 63, 69–72

Van Boxel, S., Schmidt, S., Ludwig, W., Zhang, Y.B., Sørensen, H.O., Pantleon, W., and Juul Jensen, D. (2010). Monitoring grain boundary movement during recrystallization using topo-tomography *in* N. Hansen *et. al* (ed.). Proceedings *of the 31st. Risø International Symposium on Materials Science, Risø National Laboratory, Roskilde, Denmark*.

Vaughan, G.B.M., Schmidt, S., and Poulsen, H.F. (2004), Multicrystal approach to crystal structure solution and refinement. Z. Kristall. 219**,** 813.

Vaughan, G.B.M, Wright, J.P., Bytchkov, A., Curfs, C., Gundlach, C., Orlova, M., Erra, L, Gleyzolle, H., Buslaps, T. Götz, A., Suchet, G., Petitdemange, S., Rossat, M., Margulies, L.. Ludwig, W., Snigirev, A., Snigirev, I., Schmidt, S., Sørensen, H.O., Lauridsen, E.M., Olsen, U.L., Oddershede, J., and Poulsen, H.F. (2010). The extension of ID11 for nanoscale and hierarchical characterization *in* N. Hansen *et. al* (ed.). Proceedings *of the 31st. Risø International Symposium on Materials Science, Risø National Laboratory, Roskilde, Denmark*

West, S., Schmidt, S., Sørensen, H.O., Winther, G., Poulsen, H.F., Margulies, L., Gundlach, C., and Juul Jensen, D. (2009). Direct non-destructive observation of bulk nucleation in 30% deformed aluminum. Scripta Materialia 61, 875-878.

Winther, G., Margulies, L., Schmidt, S., and Poulsen, H.F. (2004), Lattice rotations of individual bulk grains. Part 2: Correlation with initial orientation and model comparison. Acta Mater. 52, 2863-2872

Wroblewski, T., Clauss, O., Crostack, H.-A. Ertel, A., Fandrich, F., Genzel, Ch., Hradil, K., Ternes, W. and Woldt, E. (1999). A new diffractometer for materials science and imaging at HASYLAB beamline G3. Nucl. Instr. Meth. A 428**,** 570-582.